Author Manuscript

Author Manuscript

Author Manuscript

Author Manuscript

HHS Public Access

Author manuscript

Ann Biomed Eng. Author manuscript; available in PMC 2017 July 01.

Published in final edited form as:

Ann Biomed Eng. 2016 July ; 44(7): 2251–2260. doi:10.1007/s10439-015-1518-x.

Vascular response to experimental stent malapposition and under-expansion

CAROLINE C. O'BRIEN[*,1], **AUGUSTO C. LOPES**[1], **KUMARAN KOLANDAIVELU**[1,2], **MIE KUNIO**[1], **JONATHAN BROWN**[1], **VIJAYA B. KOLACHALAMA**[1,3], **CLAIRE CONWAY**[1], **LYNN BAILEY**[4], **PETER MARKHAM**[4], **MARCO COSTA**[5], **JAMES WARE**[6], and **ELAZER R. EDELMAN**[1,2]

[1]Institute of Medical Engineering and Science, Massachusetts Institute of Technology, Cambridge, MA, USA

[2]Cardiovascular Division, Brigham and Women's Hospital, Harvard Medical School, Boston, MA, USA

[3]Charles Stark Draper Laboratory, 555 Technology Square, Cambridge, MA, USA

[4]CBSET, MA, USA

[5]University Hospitals, Cleveland, OH, USA

[6]Harvard School of Public Health, Boston, MA, USA

Abstract

Background—Up to 80% of all endovascular stents have malapposed struts, and while some impose catastrophic events others are inconsequential.

Methods and Results—Thirteen stents were implanted in coronary arteries of seven healthy Yorkshire pigs, using specially-designed cuffed balloons inducing controlled stent malapposition and under-expansion. Optical coherence tomography (OCT) imaging confirmed that 25% of struts were malapposed (strut-wall distance< strut thickness) to variable extent (max. strut-wall distance *malapposed group* 0.51±0.05mm versus *apposed group* 0.09±0.05mm, p=2e-3). Imaging at follow-up revealed malapposition acutely resolved (<1% of struts remained malapposed at day 5), with strong correlation between lumen and the stent cross-sectional areas (slope =0.86, p<0.0001, R^2=0.94). OCT in three of the most significantly malapposed vessels at baseline showed high correlation of elastic lamina area and lumen area (R^2=0.96) suggesting all lumen loss was related to contraction of elastic lamina with negligible plaque/intimal hyperplasia growth. Simulation showed this vascular recoil could be partially explained by the non-uniform strain environment created from sub-optimal expansion of device and balloon, and the inability of stent support in the malapposed region to resist recoil.

Correspondence To: Dr. Caroline C. O'Brien, Institute of Medical Engineering and Science, Massachusetts Institute of Technology, 77 Massachusetts Avenue, E25-449, Cambridge, MA, USA - 02139, ; Email: ccob@mit.edu, Telephone: +1 617-253-1569, Fax: +1 617-253-2514

Author Manuscript Author Manuscript Author Manuscript Author Manuscript

Conclusions—Malapposition as a result of stent under-expansion is resolved acutely in healthy normal arteries, suggesting existing animal models are limited in replicating clinically observed persistent stent malapposition.

Keywords

Optical Coherence Tomography; Stent; Malapposition; Stent under-expansion; Pre-clinical Model

Introduction

Stent thrombosis risk arises early after implantation, can persist for years with drug-eluting stents, and is often catastrophic ([1,2]). The steady state risk, ~0.3-1% annually ([3,4]), increases in specific patient subsets ([5]), and bio-resorbable scaffolds ([6,7]), but also with inadequate stent sizing relative to vessel diameter ("stent under-expansion") ([8,9]) and lesion/vessel morphology (particularly calcified lesions) ([8,10]) as both prevent contact relative to the lumen wall. Intravascular imaging like ultrasound (IVUS) and optical coherence tomography (OCT) have improved outcomes ([11,12]) by guiding device implantation and avoiding obvious errors in placement.

We studied the impact of stent under-expansion and strut malapposition in a controlled manner in healthy porcine coronary arteries. Controlled under-expansion and malapposition were generated with bare metal stents by applying a restrictive cuff to the mid-portion of the balloon during expansion resulting in a "dogbone" shape in its expanded state. OCT imaging performed at baseline, and at post-implantation, provided information on vessel diameter, stentvessel wall apposition and tissue coverage.

Methods

Procedure

Animal procedures complied with the Guide for the Care and Use of Laboratory Animals and were approved by Institutional Animal Care and Use Committee at AAALAC accredited CBSET, Inc (Lexington, MA). Yorkshire swine (n = 8, 35-45 kg) underwent coronary artery intervention. To prevent or reduce the occurrence of thrombotic events, aspirin (650 mg, PO) and clopidogrel (300 mg, PO) were administered the day before stent implantation, and then daily at 81 and 75 mg. Animals were sedated with Telazol (4-6 mg/kg IM) and anesthetized with inhaled isoflurane under positive ventilation.

After induction of anesthesia, an 8F introducer sheath was placed aseptically in the carotid artery via cutdown approach. Heparin (150 U/kg, IV) maintained ACT greater than 275 seconds. Under fluoroscopic guidance, a 7F JL 3.5 VISTA BRITE TIP® guide catheter (Cordis Corp.) was advanced through the sheath into the ascending aorta and to the coronary arteries. Nitroglycerin (200 mg, IA) was administered into the coronary arteries and angiographic images identified proper deployment location. Bare metal stents in the left anterior descending (n=5), circumflex (n=4), and right coronary arteries (n=7), using specially designed cuffs to modify the inflation of 3.0x18 mm (W X L) balloon catheters. Two sizes of restrictive PET tubing placed over the balloon midportion 2.8×5 - or 2.5×5 mm

Author Manuscript Author Manuscript Author Manuscript Author Manuscript

upon optimal inflation (12 atm) induced constrained hourglass expansion. Balloons were deployed at balloon:artery ratios of 1-1.1 so as to ensure minimal injury and in line with current clinical convention. One vessel was excluded based on severe vascular injury (ruptured EEL) on account of balloon overexpansion and as observed by histology at necropsy (see Supplemental Figure 2). Two vessels were excluded from final analysis due to inadequate imaging resolution. The remaining 13 vessels in 7 animals (1.85 ± 0.9 stented vessels/ animals), included three fully apposed, and ten with programmed stent under-expansion with stent strut malapposition. Following deployment, angiograms were obtained (30 frames/s; paired planar cine). Frequency-Domain OCT images (C7-XR OCT Intravascular Imaging System; St. Jude Medical) were acquired immediately post-procedure and at 5-days, and 28 days. After 200 μg nitroglycerin intracoronary, the OCT catheter (C7 Dragonfly, St Jude Medical) was advanced ~5 mm distal to the stent. Acquisition was performed during power contrast flushing (4-6 mL/s for 3 seconds). Pullback was 20 mm/s for 200 μm lateral resolution initiated automatically upon blood clearance and repeated if motion artifacts or inadequate flushing occurred. After z-offset calibration, images were stored for processing. All animals were survived for 28 days, and then euthanized.

OCT Frame Analysis

Semi-automated programs allowed for simultaneous measurement of stent strut and lumen structures from OCT Frames as described previously ([13,14]) and in the supplement. Strut-level measurements on the OCT frame included **strut-wall distance**, and denote the distance of this identified strut surface relative to the lumen contour, not overlaying a side-branch. To account for strut "blooming" artifact ([15]), a strut was defined as thickness 0.1mm (0.08mm plus 0.02mm).

Stent cross-sectional area (**Stent CSA**) was measured as the area of the circle fitting the leading (abluminal edge) of the detected struts in each frame-with a minimum requirement of struts located in at least three quadrants. Lumen cross sectional area (**Lumen CSA**) was the area bounded by the luminal border. Stent and lumen CSA were measured on each frame along pullback without a sidebranch, and were validated against a subset of frames whose areas were manually obtained from the console. The difference in lumen and stent areas between the two methods were 0.42 ± 0.13 mm^2 (n = 62 frames, r = 0.97) and 0.2 ± 0.17mm^2 (n = 57 frames, r = 0.98), respectively (See Supplemental methods). The **reference lumen CSA** was defined for each vessel as the average of the baseline CSA every 1mm, for 5mm proximal and distal of stent boundaries in OCT frames ([10]). This dimension is assumed ideal expansion before remodeling but maybe affected by vasospasm. The external elastic lamina (EEL) cross-sectional area (**EEL CSA**) was manually traced in IMAGEJ by a trained operator at every 1mm of pullback. **Stent Expansion Ratio** was the ratio of stent and reference lumen CSA. Histologic evaluation determined mural injury - vessels with significant injury were excluded.

Finite Element Simulation

An *in silico* representation of the cuffed balloon and stent deployment in a porcine vessel was created using the finite element software Abaqus (v6.14, Dassault Systems, RI, USA). Literature values provided mesh, stent material ([16]) and porcine tissue properties ([17]).

Author Manuscript Author Manuscript Author Manuscript Author Manuscript

Contact between a fixed cuff and the stent was removed limiting balloon inflation in the central axial assembly region. We assumed that the contribution of blood flow to the passive elas tic tissue response in terms of loading would be negligible in comparison to the loading imposed by balloon and stent during implantation.

Histopathology

Following euthanasia at 28 days, the hearts were explanted and pressure perfused with 10% Neutral buffered formalin. Stented vessels were trimmed of myocardium and embedded in methyl methacrylate monomer (MMA) resin. Radiographs identified malapposed regions and proximal apposed, mid malapposed, and distal apposed segments. Microtomed sections were stained with Verhoffs elastin stain and Hematoxylin and eosin stain. Struts on each histopathologic section were scored for injury and inflammation on a per strut basis: 0 = no injury, Internal Elastic Lamina (IEL) intact; 1 = IEL disruption; 2 = medial disruption; and 3 = EEL/ adventitial disruption, and 0 = no inflammatory cells peristrut; 1 = < 20 cells peristrut; 2 = > 20 cells peri strut, with or without tissue effacement and little-to-no impact on tissue function; and 3 = > 20 cells peristrut with effacement of adjacent vascular tissue and adverse impact on tissue function).

Ex-vivo Deployment

Following euthanasia, a single unstented coronary vessel segment (~3.0mm diameter) was explanted and immersed in sodium chloride. A modified cuffed balloon and stent (same as used in-vivo) was prepared in the same manner as the in-vivo deployments. The vessel was placed under a stereomicroscope (VHX-1000E Keyence) and reference outer vessel dimensions were taken prior to deployment to determine proper inflation pressure as per compliance chart. Pressure was increased in 2 atmosphere increments, and high-resolution images of deployment stored for offline analysis.

Statistics

Strut and cross-sectional measurements within Stent Groups (malapposed/apposed) were compared using Student's t-test, and, when normality could not be supported, the Mann-Whitney Test. As hierarchical design was used a linear mixed effects model (LME) tested for associations between covariates and control for nesting of measurements within animal and vessel. In-vessel characteristics (e.g. stent CSA) were treated as fixed effects, while animal and vessel were treated as random effects in an LME, fitted using maximum likelihood estimation. The contribution of one covariate model in the presence of other covariates was tested using the log-likelihood ratio test for nested measurements. $p < 0.05$ was statistically significant. Where piecewise linear regression models were employed (as in Figure 4), optimal location of knots was chosen based on minimizing the deviance in the LME. R^2 was measure of association. All analyses were performed using R version 2.12.1.

Results

Benchtop verification of method of controlled under-expansion of the stent

Prior to deployment in animals, the method of graded under-expansion and malapposition was characterized computationally using an ex-vivo setup. Finite element methods simulated

Author Manuscript Author Manuscript Author Manuscript Author Manuscript

(Figure 1A) deployment of a stent cuffed-balloon inflated. At low inflation pressures, the device expands first proximal and distal to dimensions larger than the inner diameter of the vessel (10% balloon oversizing ensured device anchoring without deep tissue injury). Radial stretch pulled tissue at its margins, creating axial tensile strain in the middle, under-expanded segment, and subsequent luminal shrinkage (~0.03 mm radial inwards displacement at mid-point). Luminal shrinkage at full inflation was still so small that lumen diameter remained significantly larger than cuffed balloon diameter – indicating strut malapposition and stent under-expansion. Stent foreshortening was less than 2%. Ex-vivo cuffed-balloon inflation of a stent to nominal pressure in an explanted coronary artery followed the finite element simulation (Figure 1C) with the vessel over-expanded subtly proximally (Figure 1B) and distally, and the vessel shrank in diameter ~10% in the mid, under-expanded regions.

In-vivo Deployment of Under-expanded Devices and Serial Imaging Study

Implant—QCA balloon-artery ratios (Figure 2A) were as predicted for all balloon cuff sizes (mean difference in balloon-artery ratio predicted vs. actual = 0.07 ± 0.05, p=0.01; Table I).

As assessed from OCT (Figure 2B, table II), deployment of devices on cuffed balloons created ranges of stent expansion and strut-wall apposition (Figure 2C) that met the criteria of both stent under-expansion (stent CSA/reference lumen area <0.8 ([18])) and malapposition (strut-wall distance ≤0.1, corresponding to one strut thickness). Vessels were reclassified into *as-treated* malapposed (95% maximum strut-wall distance >0.1, n=10 stents) and apposed stent groups (n=3 stents).

At baseline, lumen area correlated with stent area (Figure 4 in blue; R^2=0.86), though differently for underexpanded and fully expanded stents. Piecewise linear mixed effects models fit to lumen and stent cross sectional dimensions found an optimal knot at stent expansion ratio of 86.8%. Above stent expansions ratio of 86.8%, the lumen dilated with expansion (β=0.40; 95% CI (0.25,0.71); p <0.0001) - below the lumen dilated with decreasing stent expansion (β=− 0.25; 95% CI (−0.31,−0.21); p <0.0001), indicating acute dilation in the middle, under-expanded region, as visualized in single vessel reconstructions (Fig 3A). For a nominal stent size of 3.0mm, this threshold ratio corresponds to mean stent area of 6.0mm^2 which is not significantly different from previously identified thresholds of clinically relevant stent under-expansion ([18],[19]).

Follow-up—At 5 days follow-up, there was recovery of malapposition across all vessels. <1% of struts remained malapposed, 36% had no coverage, and 95% <0.08mm of overlying nascent tissue hyperplasia (or fibrin) (less than a strut width). The lumen dimension converged to stent dimension with strong linear correlation (average slope β=0.86; 95% CI (0.82,0.89); p <0.0001, R^2=0.94, Figure 4 in red). For a single vessel with significant stent under-expansion, this is visualized as a constriction in the middle portion (Figure 3B).

Mean stent CSA decreased between baseline and follow up for the entire sample (6.79 ± 0.75 mm^2 at day 0 versus 6.43 ± 0.67 mm^2 at day 5, p <0.0001, Mann-Whitney), indicating minimal stent recoil between 0 and 5 days (~ 5%).

Author Manuscript Author Manuscript Author Manuscript Author Manuscript

Observations at day 5 of luminal conformation onto the under-expanded stent were reasonably explained by elastic recoil (Figure 5): with lumen cross-sectional area correlating with external elastic lamina cross-sectional area (manually traced from OCT in three of the most extreme under-expanded stents) indicating recoil of the elastic lamina driving this luminal shrinkage. There was minimal evidence of plaque or intimal hyperplasia growth to explain reduction in lumen area at malapposition sites.

Histopathology

Histopathology at necropsy (28 days) revealed no malapposed struts, little evidence of excessive injury or inflammation. 707 of struts were analyzed in 45 sections. All were in contact with the media; 97% of struts with IEL intact and compressed media, and the remaining 3% having lacerated IEL, compressed media but with EEL still intact. Inflammation was also low; 60% of struts had no inflammatory cells and the remaining 40% had fewer than 20 cells, without tissue effacement and little to no impact on tissue function.

OCT-derived neointimal area measured at day 28 and histopathology-derived neointimal area at necropsy of each of the vessels used in the study showed acceptable agreement in segment-matched means (OCT, $R^2 = 0.66$). The regression line was OCT= 0.60* histo + 1.05.

Discussion

The first experimental model of stent malapposition and under-expansion

Strut-level complications within stents from clinical trials are associated with strut-wall displacement ([20],[21]) and altered flow ([22]). We created a novel model of reproducibly controlling stent malapposition through stent under-expansion; by deploying stents mounted on hourglass shaped balloons inducing both acute strut displacement from the wall (malapposition) of up to 600 microns, and up to 40% under-inflation - values consistent with clinical reports ([20]). While both malapposition and under-expansion can occur simultaneously, one should dominate. Under-expansion without acute strut malapposition would occur when plaque features preclude optimal stent expansion (e.g. calcium nodules). Likewise malapposition can occur with 'optimal' stent expansion - as in vascular taper, where we commonly see malapposition at the proximal edges of stents, or at bifurcations where the vessel is "healthy" without injury and or plaque. A limitation extrapolating these results to the clinic is that this model had malapposed struts in the middle of the stents in stretched vessels-whereas acute malapposition is mostly observed at stent edges. We leveraged high resolution imaging from fusion imaging, enabling us to follow the device, tissue response at follow-up time points. With this sophisticated experimental architecture in place, we examined the impact of stent malapposition and under-expansion through presumably natural environmental drivers such as altered flow and procedure-induced structural changes. However, early observations from intravascular imaging at day 5 and before any presumed tissue response were unexpected and intriguing, and forced us to orient our attention on acute morphologic changes in the arterial wall.

Author Manuscript Author Manuscript Author Manuscript Author Manuscript

Healthy vessel response to acute stent under-expansion is recoil

The early reaction to under-expanded and malapposed devices was lumen dilation followed by contraction of the wall onto the under-expanded stent. Benchtop and computational simulation of this sub-optimal deployment revealed that this sub-acute lumen dilation (up to 20 % lumen area increase) in regions of under-expansion could partially be explained by passive elastic forces of the vessel during incomplete balloon expansion. On a tri-folded cuffed balloon, the balloon and stent expands ends first. With serial inflation of the balloon and stent to nominal pressure (~14atm) the healthy vessel will compensate by stretching outwards and pull axially inwards at its margins. Non-uniform expansion creates tensile axial strain in the middle region, contributing to subtle luminal shrinkage (radial strain). In-vitro, ex-vivo and computational simulations confirmed acute luminal shrinkage and axial tensile strain. OCT confirmed in-vivo luminal dilation (~20%) following incomplete expansion of the device. With no evidence of a passive mechanical event driving this acute vaso dilation (Figure 1A), this is likely a vasomotor effect.

Though small, sub-acute radial dilation in the under-expanded region is likely the nidus for subsequent recoil onto the stent. The amount of vascular recoil observed here - up to 40% area decrease - is not unprecedented given earlier experience with balloon angioplasty ([23,24]), however was not expected in the context of an under-expanded stent especially as there was no significant balloon injury in this region with overstretch since the balloon failed to contact the wall. Recoil almost completely restored apposition at day 5, even as >25% of all struts were initially malapposed. In response to stent under-expansion, the healthy swine vessel will recoil quickly, in advance of any tissue response, resolving any stent-wall malapposition. Without any significant malapposition at early acute time-point- and still *ahead* of any tissue response, we could not create the baseline condition necessary to identify the role of malapposition in neointimal response.

Utility of healthy animal models to study real-world implants

Animal models offer control over multiple parameters and environments that cannot be achieved in the heterogeneity of the clinic, and the living dynamic lacking on the bench. Healthy porcine coronary vessel arteries are routinely used pre-clinically in both early stage device development, late regulatory approval. Yet, there is a tension in use of the animal – the naïve healthy state maximizes synchrony and consistency of results and reveals important basic biological reparative mechanisms ([25,26]) but may include compensatory responses and reflexes muted or absent in disease. The uninjured or native state in the animal may not fully represent the pathologic condition. This we observed; the healthy vessel recoils almost immediately onto malapposed struts, before tissue response. Intact elasticity, smooth muscle cell architecture and vascular health restores vessel homeostasis impossible clinically. Though daily administration of a vasodilator (calcium channel blocker) might reduce the vasopressive response and recoil around the struts, this may cause even further departure from the clinical reality. Malapposition does persist in bare metal ([27]) and drug-eluting devices ([20,28]) in patients but cannot in the intact arteries of normal animals. There is a paucity of clinical studies evaluating this phenomenon serially using matched strut-level analysis after drug-eluting stent implantation, precluding definitive conclusion on acute malapposition resolution in humans with coronary disease. It is possible

Author Manuscript Author Manuscript Author Manuscript Author Manuscript

that all malapposed stents resolve but new ones are formed due to incompletely understood drug-stent-vessel interaction ([29]). Acute malapposition is thus quickly resolved or, more likely, impossibly modeled in the healthy vessel. The presence of a lesion - which almost always precedes a stent implant - will limit the normal vessels ability to elastically recoil ([30]), and is a known risk factor for acute malapposition ([31]).

It is likely that this compensation is increasingly lost in the face of disease. Animal models with normal and intact arteries are thus fine substrates to determine patterns of vascular response to device insertion in native arteries-everything observed in the intact vessel emerges de novo allowing for an orderly definition of sequential physiologic repair-but they may not be ideal for defining and understanding aberrant responses. This fundamental difference in physiologic compensation and pathologic decompensation could explain the divergence in preclinical models and clinical experience with DES. This is even more so the case now with novel interventional devices, including the bio-resorbable and bio-erodible scaffolds, wherein event worst outcomes have been observed ([6,7]). The issues of strut underexpansion and malapposition become even more important when considering the emerging technologies with erodible platforms. These devices maybe more prone to recoil and less apt to appose especially in diseased vessels with significant calcific burden. For this reason, as the new implantation devices evolve, so must the animal models for evaluating their procedural success, and foretelling the clinical outcomes. The present animal models must be adapted according to the environment dictated by the biological factors in realistic clinical practices. The animal models, if successfully translated, have the potential to predict the adverse outcomes and prevent the costly clinical events for latest complex implants.

It is important to note that this pre-clinical study utilized a level of analysis unprecedented including frequency-domain OCT imaging at baseline and at follow-up time, along with high fidelity imaging analysis of each acquired OCT frame. The spatial and temporal resolution of this pre-clinical vascular response is far beyond what could be appreciated or has been implemented clinically, as far as we are aware. With two sub-acute imaging time-points (post procedure and 5 days), we observed a dynamic event ahead of any tissue response that would be reasonably missed in other clinical trial imaging protocols.

Conclusions

In a healthy porcine model, vascular reaction to recover stent under-expansion and malapposition is earlier than anticipated, comprising full vessel recoil in response to an acute strain from suboptimal expansion of the balloon and device. Healthy vessels may not recapitulate the basis for vascular response in disease-laden vessels, and their utility in modeling real-world implants needs to be carefully considered.

Supplementary Material

Refer to Web version on PubMed Central for supplementary material.

Author Manuscript Author Manuscript Author Manuscript Author Manuscript

Acknowledgements

Work was supported by a grant from the NIH (R01 GM-49039) to ERE. KK is supported in part by an AHA FTF Award (12FTF12080241). MC is a consultant (speaker bureau) for Abbott and Medtronic (minor, < 10,000).

References

1. Stone GW, Rizvi A, Newman W, Mastali K, Wang JC, Caputo R, Doostzadeh J, Cao S, Simonton CA, Sudhir K, Lansky AJ, Cutlip DE, Kereiakes DJ. Everolimus-eluting versus paclitaxel-eluting stents in coronary artery disease. N. Engl. J. Med. 2010; 362:1663–74. [PubMed: 20445180]
2. Iakovou I, Schmidt T, Bonizzoni E, Ge L, Sangiorgi GM, Stankovic G, Airoldi F, Chieffo A, Montorfano M, Carlino M, Michev I, Corvaja N, Briguori C, Gerckens U, Grube E, Colombo A. Incidence, predictors, and outcome of thrombosis after successful implantation of drug-eluting stents. JAMA. 2005; 293:2126–30. [PubMed: 15870416]
3. Windecker S, Meier B. Late coronary stent thrombosis. Circulation. 2007; 116:1952–65. [PubMed: 17965406]
4. Nakazawa G, Finn AV, Joner M, Ladich E, Kutys R, Mont EK, Gold HK, Burke AP, Kolodgie FD, Virmani R. Delayed arterial healing and increased late stent thrombosis at culprit sites after drug-eluting stent placement for acute myocardial infarction patients: an autopsy study. Circulation. 2008; 118:1138–45. [PubMed: 18725485]
5. Baran KW, Lasala JM, Cox DA, Song A, Deshpande MC, Jacoski MV, Mascioli SR. A clinical risk score for prediction of stent thrombosis. Am. J. Cardiol. 2008; 102:541–5. [PubMed: 18721509]
6. Capodanno D, Gori T, Nef H, Latib A, Mehilli J, Lesiak M, Caramanno G, Naber C, Di Mario C, Colombo A, Capranzano P, Wiebe J, Araszkiewicz A, Geraci S, Pyxaras S, Mattesini A, Naganuma T, Munzel T, Tamburino C. Percutaneous coronary intervention with everolimus-eluting bioresorbable vascular scaffolds in routine clinical practice: early and midterm outcomes from the European multicentre GHOST-EU registry. EuroIntervention. 2014
7. Kraak RP, Hassell ME, Grundeken MJ, Koch KT, Henriques JP, Piek JJ, Baan J Jr. Vis MM, Arkenbout EK, Tijssen JG, de Winter RJ, Wykrzykowska JJ. Initial experience and clinical evaluation of the Absorb bioresorbable vascular scaffold (BVS) in real-world practice: the AMC Single Centre Real World PCI Registry. EuroIntervention. 2014
8. Fujii K, Carlier SG, Mintz GS, Yang YM, Moussa I, Weisz G, Dangas G, Mehran R, Lansky AJ, Kreps EM, Collins M, Stone GW, Moses JW, Leon MB. Stent underexpansion and residual reference segment stenosis are related to stent thrombosis after sirolimus-eluting stent implantation: an intravascular ultrasound study. J Am Coll Cardiol. 2005; 45:995–8. [PubMed: 15808753]
9. Cheneau E, Leborgne L, Mintz GS, Kotani J, Pichard AD, Satler LF, Canos D, Castagna M, Weissman NJ, Waksman R. Predictors of subacute stent thrombosis: results of a systematic intravascular ultrasound study. Circulation. 2003; 108:43–7. [PubMed: 12821553]
10. Liu X, Doi H, Maehara A, Mintz GS, Costa Jde R Jr. Sano K, Weisz G, Dangas GD, Lansky AJ, Kreps EM, Collins M, Fahy M, Stone GW, Moses JW, Leon MB, Mehran R. A volumetric intravascular ultrasound comparison of early drug-eluting stent thrombosis versus restenosis. JACC Cardiovasc Interv. 2009; 2:428–34. [PubMed: 19463466]
11. Prati F, Di Vito L, Biondi-Zoccai G, Occhipinti M, La Manna A, Tamburino C, Burzotta F, Trani C, Porto I, Ramazzotti V, Imola F, Manzoli A, Materia L, Cremonesi A, Albertucci M. Angiography alone versus angiography plus optical coherence tomography to guide decision-making during percutaneous coronary intervention: the Centro per la Lotta contro l'Infarto-Optimisation of Percutaneous Coronary Intervention (CLI-OPCI) study. EuroIntervention : journal of EuroPCR in collaboration with the Working Group on Interventional Cardiology of the European Society of Cardiology. 2012; 8:823–9.
12. Ahn JM, Kang SJ, Yoon SH, Park HW, Kang SM, Lee JY, Lee SW, Kim YH, Lee CW, Park SW, Mintz GS, Park SJ. Meta-analysis of outcomes after intravascular ultrasound-guided versus angiography-guided drug-eluting stent implantation in 26,503 patients enrolled in three randomized trials and 14 observational studies. The American journal of cardiology. 2014; 113:1338–47. [PubMed: 24685326]

Author Manuscript Author Manuscript Author Manuscript Author Manuscript

13. Ughi GJ, Adriaenssens T, Onsea K, Kayaert P, Dubois C, Sinnaeve P, Coosemans M, Desmet W, D'Hooge J. Automatic segmentation of in-vivo intra-coronary optical coherence tomography images to assess stent strut apposition and coverage. Int. J. Cardiovasc. Imaging. 2012; 28:229–41. [PubMed: 21347593]

14. Tsantis S, Kagadis GC, Katsanos K, Karnabatidis D, Bourantas G, Nikiforidis GC. Automatic vessel lumen segmentation and stent strut detection in intravascular optical coherence tomography. Med. Phys. 2012; 39:503–13. [PubMed: 22225321]

15. Bezerra HG, Costa MA, Guagliumi G, Rollins AM, Simon DI. Intracoronary optical coherence tomography: a comprehensive review clinical and research applications. JACC Cardiovasc Interv. 2009; 2:1035–46. [PubMed: 19926041]

16. Conway C, Sharif F, McGarry JP, McHugh PE. A Computational Test-Bed to Assess Coronary Stent Implantation Mechanics Using a Population-Specific Approach. Cardiovasc Eng Tech. 2012; 3:374–387.

17. Lally C, Reid AJ, Prendergast PJ. Elastic behavior of porcine coronary artery tissue under uniaxial and equibiaxial tension. Ann Biomed Eng. 2004; 32:1355–64. [PubMed: 15535054]

18. de Jaegere P, Mudra H, Figulla H, Almagor Y, Doucet S, Penn I, Colombo A, Hamm C, Bartorelli A, Rothman M, Nobuyoshi M, Yamaguchi T, Voudris V, DiMario C, Makovski S, Hausmann D, Rowe S, Rabinovich S, Sunamura M, van Es GA. Intravascular ultrasound-guided optimized stent deployment. Immediate and 6 months clinical and angiographic results from the Multicenter Ultrasound Stenting in Coronaries Study (MUSIC Study). Eur. Heart J. 1998; 19:1214–23. [PubMed: 9740343]

19. Sonoda S, Morino Y, Ako J, Terashima M, Hassan AH, Bonneau HN, Leon MB, Moses JW, Yock PG, Honda Y, Kuntz RE, Fitzgerald PJ, Investigators S. Impact of final stent dimensions on long-term results following sirolimus-eluting stent implantation: serial intravascular ultrasound analysis from the sirius trial. J Am Coll Cardiol. 2004; 43:1959–63. [PubMed: 15172398]

20. Gutierrez-Chico JL, Wykrzykowska J, Nuesch E, van Geuns RJ, Koch KT, Koolen JJ, di Mario C, Windecker S, van Es GA, Gobbens P, Juni P, Regar E, Serruys PW. Vascular tissue reaction to acute malapposition in human coronary arteries: sequential assessment with optical coherence tomography. Circ Cardiovasc Interv. 2012; 5:20–9. S1-8. [PubMed: 22319063]

21. Sera F, Awata M, Uematsu M, Kotani J, Nanto S, Nagata S. Optimal stent-sizing with intravascular ultrasound contributes to complete neointimal coverage after sirolimus-eluting stent implantation assessed by angioscopy. JACC Cardiovasc Interv. 2009; 2:989–94. [PubMed: 19850260]

22. Foin N, Gutierrez-Chico JL, Nakatani S, Torii R, Bourantas CV, Sen S, Nijjer S, Petraco R, Kousera C, Ghione M, Onuma Y, Garcia-Garcia HM, Francis DP, Wong P, Di Mario C, Davies JE, Serruys PW. Incomplete stent apposition causes high shear flow disturbances and delay in neointimal coverage as a function of strut to wall detachment distance: implications for the management of incomplete stent apposition. Circ Cardiovasc Interv. 2014; 7:180–9. [PubMed: 24642998]

23. Schoenhagen P, Ziada KM, Vince DG, Nissen SE, Tuzcu EM. Arterial remodeling and coronary artery disease: the concept of "dilated" versus "obstructive" coronary atherosclerosis. J Am Coll Cardiol. 2001; 38:297–306. [PubMed: 11499716]

24. Rodriguez AE, Palacios IF, Fernandez MA, Larribau M, Giraudo M, Ambrose JA. Time course and mechanism of early luminal diameter loss after percutaneous transluminal coronary angioplasty. Am. J. Cardiol. 1995; 76:1131–4. [PubMed: 7484897]

25. Schwartz RS, Edelman E, Virmani R, Carter A, Granada JF, Kaluza GL, Chronos NA, Robinson KA, Waksman R, Weinberger J, Wilson GJ, Wilensky RL. Drug-eluting stents in preclinical studies: updated consensus recommendations for preclinical evaluation. Circ Cardiovasc Interv. 2008; 1:143–53. [PubMed: 20031669]

26. Schwartz RS, Edelman ER, Carter A, Chronos N, Rogers C, Robinson KA, Waksman R, Weinberger J, Wilensky RL, Jensen DN, Zuckerman BD, Virmani R, Consensus C. Drug-eluting stents in preclinical studies: recommended evaluation from a consensus group. Circulation. 2002; 106:1867–73. [PubMed: 12356643]

27. van der Hoeven BL, Liem SS, Dijkstra J, Bergheanu SC, Putter H, Antoni ML, Atsma DE, Bootsma M, Zeppenfeld K, Jukema JW, Schalij MJ. Stent malapposition after sirolimus-eluting and bare-metal stent implantation in patients with ST-segment elevation myocardial infarction:

Author Manuscript Author Manuscript Author Manuscript Author Manuscript

acute and 9-month intravascular ultrasound results of the MISSION! intervention study. JACC Cardiovasc Interv. 2008; 1:192–201. [PubMed: 19463300]

28. Im E, Kim BK, Ko YG, Shin DH, Kim JS, Choi D, Jang Y, Hong MK. Incidences, predictors, and clinical outcomes of acute and late stent malapposition detected by optical coherence tomography after drug-eluting stent implantation. Circ Cardiovasc Interv. 2014; 7:88–96. [PubMed: 24425586]
29. Guagliumi G, Bezerra HG, Sirbu V, Ikejima H, Musumeci G, Biondi-Zoccai G, Lortkipanidze N, Fiocca L, Capodanno D, Wang W, Tahara S, Vassileva A, Matiashvili A, Valsecchi O, Costa MA. Serial Assessment of Coronary Artery Response to Paclitaxel-Eluting Stents Using Optical Coherence Tomography. Circulation-Cardiovascular Interventions. 2012; 5:30–38. [PubMed: 22298797]
30. Rensing BJ, Hermans WR, Strauss BH, Serruys PW. Regional differences in elastic recoil after percutaneous transluminal coronary angioplasty: a quantitative angiographic study. J Am Coll Cardiol. 1991; 17:34B–38B.
31. Tanigawa J, Barlis P, Di Mario C. Heavily calcified coronary lesions preclude strut apposition despite high pressure balloon dilatation and rotational atherectomy: in-vivo demonstration with optical coherence tomography. Circ. J. 2008; 72:157–60. [PubMed: 18159118]

Author Manuscript Author Manuscript Author Manuscript Author Manuscript

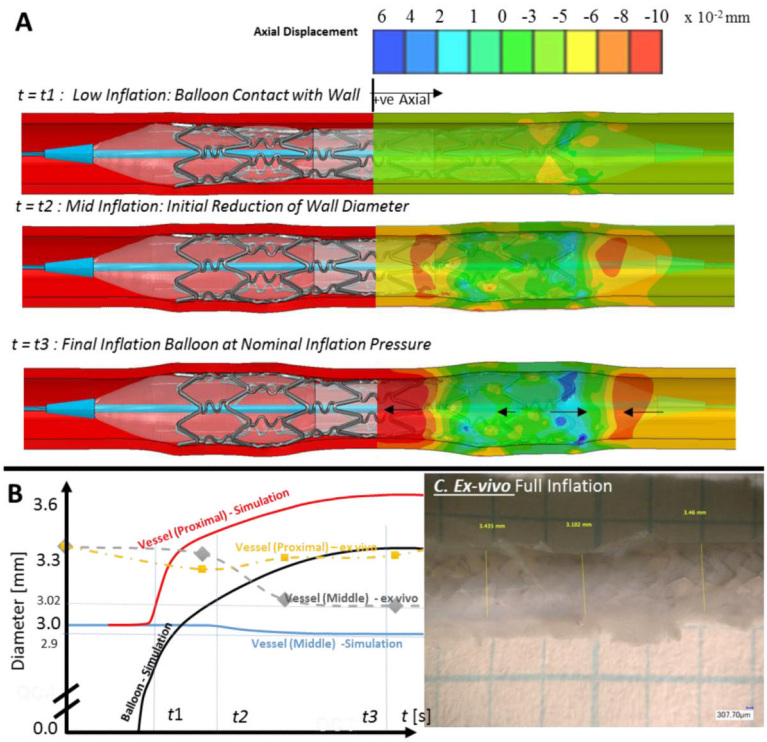

Figure 1.

(A) Finite-element simulation show that at low inflation pressures the cuffed tri-folded balloon expands first in the extremities of the device slightly larger than the inner diameter of the vessel. The vessel must compensate by (B) stretching radially outwards, pulling tissue at margins inwards creating axial strain. For the middle region, the expansion of the device in proximal and distal regions creates axial tensile strain. At some time-point t_2, this axial strain caused a negative radial strain (inward) of ~2% (0.05mm radial inwards displacement) at this midpoint. (C) Ex-vivo deployment of the generic stent (used animal study) in an explanted swine coronary artery of 3.1mm inner diameter (3.3mm outer diameter), shows that nominal inflation the device created some overstretch in the proximal and distal segments, and partial shrinkage in the middle segment indicating a lumen diameter and cross-sectional area shrinkage of 3% and 6%.

Author Manuscript Author Manuscript Author Manuscript Author Manuscript

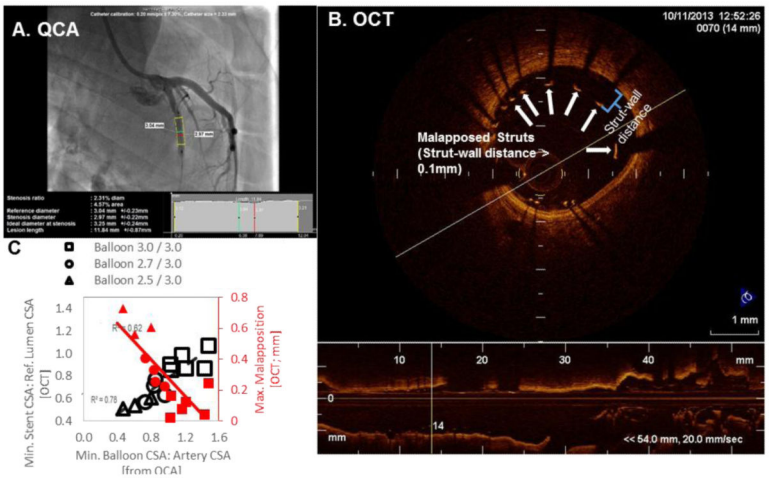

Figure 2.

The expansion of the modified balloon (**A**; from QCA), generated ranges of stent under-expansion (B; min stent /reference lumen CSA) and malapposition (**B**; maximum strut-wall displacement within the stent by OCT), in all 13 vessels analyzed (C). Note struts with Wall Distance >0.1mm are malapposed.

Author Manuscript Author Manuscript Author Manuscript Author Manuscript

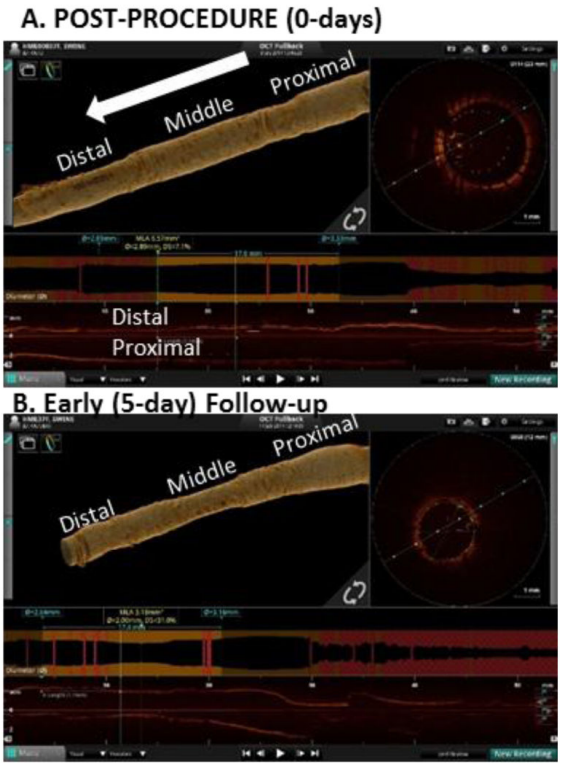

Figure 3.

Volume rendered reconstructions of the lumen using proprietary off-line analysis (St. Jude) for a vessel implanted with 2.5mm/3.0mm cuff and achieving a minimum stent expansion ratio (stent/reference lumen CSA) of 50.7% at baseline. (A) At baseline, the lumen appears dilated in middle under-expanded segment, which then (B) recoils onto the stent as observed at early (5 day) follow-up.

Author Manuscript Author Manuscript Author Manuscript Author Manuscript

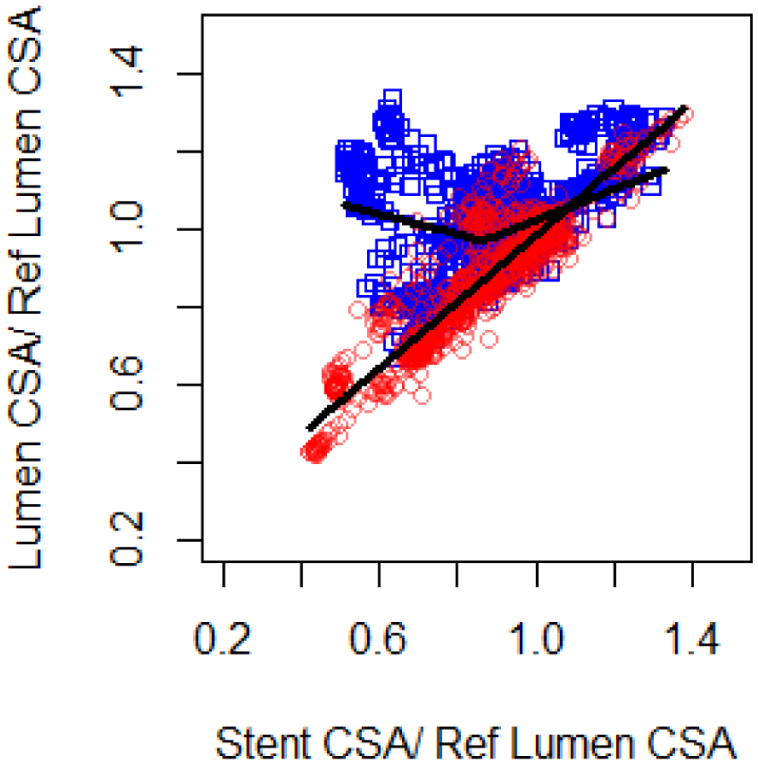

Figure 4.

Normalized lumen CSA (lumen-to-mean vessel reference lumen area ratio) versus stent expansion ratio (stent-to-mean vessel reference lumen area ratio) at baseline (blue) and follow up (red), with piecewise linear regression lines plotted of the fixed effects estimates after adjustment for measurements nested in vessels and animals.. For day 0 optimal knots in the piecewise linear model were found at stent expansion ratio = 0.86 (Stent expansion ratio = 86%; $R^2 = 0.85$). Follow-up showed strong, linear and positive correlation between stent and lumen cross-sections ($R^2 = 0.94$).

Author Manuscript Author Manuscript Author Manuscript Author Manuscript

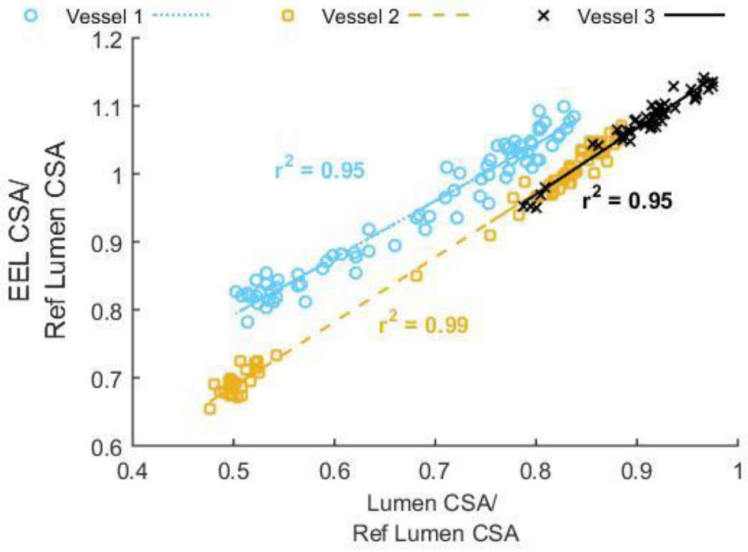

Figure 5.

Luminal area shrinkage follows vessel elastic recoil as determined by mapping the lumen cross-sectional area to the EEL cross sectional area manually traced in OCT frames of three of the extremely malapposed vessels (malapposition at baseline >4*strut-widths). Lumen and EEL CSA normalized to the reference non-stented lumen dimension in each vessel correlated with near unity linear regression slopes close to 1 ($\beta_{vessel\ 1}$ = 0.84 (blue), $\beta_{vessel\ 2}$ = 0.95 (yellow), $\beta_{vessel\ 3}$ = 0.97 (black)).

Author Manuscript

Author Manuscript

Author Manuscript

Author Manuscript

Table I

Balloon Artery Ratio: QCA v. Predicted

Balloon Middle / Proximal	***n***	**Pressure [Pa]**	**Vessel Diameter *From QCA* [mm]**	**Min. Balloon/Artery Ratio *From QCA* [mm / mm]**	**Min. Balloon/Artery Ratio *As predicted* [mm / mm]**
3.0 / 3.0	6	11.50 ± 2.51	2.81 ± 0.18	1.13 ± 0.08	1.05 ± 0.03
2.7/3.0	4	1025 ± 0.50	2.84 ± 0.07	1.01 ± 0.02	0.95 ± 0.02
2.5 /3.0	3	15.00 ± 1.00	2.90 ± 0.17	0.87 ± 0.11	0.88 ± 0.05

Shown as mean ± st. dev

Author Manuscript Author Manuscript Author Manuscript Author Manuscript

Table II

OCT measurements in stent groups at baseline and follow-up

		Treatment Group		
		Malapposed	**Apposed**	
	Number	**10**	**3**	***p*-value**
OCT	***Cross-Sectional Measures***			**** significant at the 5% level***
Baseline	Mean Reference Lumen CSA [mm2]	7.50 ± 1.10	6.51 ± 0.56	0.0747
	Mean Stent CSA [mm2]	6.30 ± 0.47	6.95 ± 0.96	0.5059
	Stent Overexpansion [Max Stent CSA / Mean Lumen Ref CSA]	1.00 ± 0.14	1.18 ± 0.11	0.0878
	Stent Underexpansion [Min Stent CSA / Mean Lumen Ref CSA]	0.71 ± 0.18	0.92 ± 0.06	0.0102 *
	Strut-Level Measures			
	Number of Struts	6955	1469	
	Number of Malapposed Struts	2153	11	
	Number of Apposed Struts	4802	1458	
	Max Wall Distance [mm]	0.51 ± 0.23	0.09 ± 0.05	0.0002 *
	Mean Wall Distance [mm]	0.11 ± 0.08	−0.02 ± 0.01	0.0070 * *Mann-Whitney*
Acute [5 days]	Number of Struts	6366	1289	
	Number of Malapposed Struts	27	2	
	Number of Apposed Struts	6339	1287	
	Max Wall Distance [mm]	0.15 ± 0.06	0.09 ± 0.05	0.1612
	Mean Wall Distance [mm]	−0.01 ± 0.01 +	−0.01 ± 0.02	0.9909
	Mean Stent CSA [mm^2]	6.03 ± 0.50 +	6.46 ± 0.45 +	0.2357
	Stent Underexpansion [Min Stent CSA / Mean Lumen Ref CSA]	0.66 ± 0.18 +	0.87 ± 0.05	0.0078 *

*significant at the 5% level

+Different to Baseline at 5% level of significance